Scanning Tunneling Microscopy Study of Thin PTCDI Films on Ag/Si(111)-√3×√3

C. Emanuelsson, H. M. Zhang, E. Moons and L. S. O. Johansson
Department of Engineering and Physics, Karlstad University, SE-651 88 Karlstad, Sweden

Abstract

3,4,9,10-perylene tetracarboxylic diimide molecules were evaporated onto a Ag/Si(111)-√3×√3 surface and studied by scanning tunneling microscopy/spectroscopy and low energy electron diffraction (LEED). The growth mode was characterized as layer-by-layer growth with a single molecular unit cell in a short range order. The growth of the first two monolayers involves a molecule/substrate superstructure and a molecule/molecule superstructure. At higher coverages the molecules in each layer were found to align so that unit cells are on top of each other. The experimentally obtained LEED pattern is described as a combination of patterns from the molecular unit cell and the molecule/substrate superstructure. The electronic structure was found to be strongly dependent on the film thickness for the first few layers: Several extra states are found at low coverages compared to higher coverages resulting in a very small pseudo gap of 0.9 eV for the first layer, which widens up to 4.0 eV for thicker films.

1 Introduction

The last few decades organic semiconductors, and thin films of these, have attracted attention as they have been proven to be viable alternatives for conventional semiconductors in several electronical applications. Organic thin films have been used to create light emitting diodes [1] field effect transistors [2], solar cells [3], photodetectors [3], organic lasers [4], chemical- and biological sensors [5]. These devices are all made of different layers of organic molecular films, conventional semiconductors and metals. The performance of these devices is highly dependent on the structure and quality of the organic films and the characteristics of the

interface between the films and other materials in the devices. Therefore, a good understanding of the properties of thin films of organic semiconductors on various substrates is important for their use in electrical devices.

The organic semiconductor 3,4,9,10-perylene tetracarboxylic diimide (PTCDI) has recently attracted attention because it can be functionalized by exchanging hydrogens on the imide groups or the perylene core with other groups to tune its electrical, optical and charge-transport properties [6]. It has been shown that the planar PTCDI molecule and some of its derivatives adsorb flatly laying and form ordered structures on several surfaces, such as metals [7–13], graphite, MoS_2 [14] and NaCl(001) [15]. So far three structures of PTCDI have been observed at room temperature (RT): “canted”, “brick wall” and “domino”. The most common structure is the “canted” structure that is constructed by rows of molecules. The molecules in every other row are slightly differently oriented relative to the row direction. The “brick-wall” structure has been observed on both Au(111) and NaCl(001). In this structure molecules also grow in rows, but all molecules have the same orientation and molecules in adjacent rows are shifted in position along the row direction. The last RT reconstruction is the “domino” structure, where the molecules bind by their edges in a square pattern, like domino bricks, leaving an opening inside the square [13]. Yet another structure has been found on Au(111) by annealing the sample at 50 °C after the PTCDI evaporation. The post annealing structure is similar to the canted one, but here the rows combine into double rows, where the molecules are oriented in the same way. These double rows are separated by a single row with differently oriented molecules [10]. Density Functional Theory (DFT) calculations of PTCDI in gas phase (without substrate) have been performed by Mura et al. [13] to explain the interactions among molecules which can lead to different stable structures. In the DFT study it was found that among the structures that have been observed in STM, the canted one was the most stable

followed by the domino- and then the brick wall structure. The stability of the canted structure comes from that the rows are made by the strongest possible PTCDI dimers. The structure is further stabilized by extra hydrogen bonding between molecules in neighboring rows. The stronger interaction along the rows is N-H···O hydrogen bonding mediated by the imide groups. The weaker interactions between rows are hydrogen bonding between the oxygen, not involved in the stronger interaction, and hydrogen of the perylene core of a neighboring PTCDI. These two interactions are possible because the molecules in adjacent rows have slightly different orientations relative to the row direction.

The metal-induced Ag/Si(111)-√3×√3 reconstruction has a hexagonal structure composed of Si- and Ag trimers [16]. The reconstruction is described by the inequivalent triangle model (IET) with two differently sized Ag trimers [17]. The surface has been shown to be weakly interacting, allowing molecules to remain mobile and interact with each other to create well-ordered layers. Well-ordered organic films have been reported on this substrate for several organic molecules, for instance, pentacene, [18] 3,4,9,10-perylene tetracarboxylic dianhydrid (PTCDA) [19,20], naphthalene tetracarbocylic dianhydride (NTCDA) and naphthalene tetracarbocylic diimide (NTCDI) [21]. The Ag/Si(111)-√3×√3 surface has also been used to create supramolecular networks of PTCDI and melamine. The networks are formed by hydrogen bonding between the melamine and the imide groups in PTCDI, creating a hexagonal structure with melamine in the corners and PTCDI at the sides [22]. The molecular organization of PTCDI on the Ag/Si(111)-√3×√3 surface has previously been studied by scanning tunneling microscopy (STM) for low coverages, < 0.5 monolayers (ML), by Swarbrick et al. [19]. It was shown that PTCDI grew in 1D rows below 0.02 ML coverage but formed 2D islands at higher coverages. These islands had the aforementioned canted structure and the molecular rows were oriented ±12º relative to the [11$\bar{2}$] direction of the substrate. However, the growth

of a complete first PTCDI layer and the growth of succeeding layers on Ag/Si(111)-√3×√3 has not yet been studied.

Here the growth of thin PTCDI films on the Ag/Si(111)-√3×√3 substrate has been studied with several PTCDI coverages from 0.1 ML up to 5 ML. Each of these coverages was studied using STM, scanning tunneling spectroscopy (STS) and low energy electron diffraction (LEED).

2 Experimental details

The experiment was conducted using an ultra-high vacuum system with separate preparation and analysis chambers. The analysis chamber was equipped with an Omicron VT STM using a W/Ir tip and an Omicron SPECTALEED. The base pressures in the analysis- and preparation chambers were 9×10^{-11} mbar and 5×10^{-11} mbar respectively. The sample used was a Shiraki-etched [23] Si(111), Sb-doped to a resistivity of 1-10 Ωcm. The oxide was removed by stepwise resistant heating up to 940 °C. The Ag/Si(111)-√3×√3 reconstruction was created by evaporating 1 ML Ag onto the substrate and annealing it at 600 °C for 2 min. LEED investigation of the surface showed a sharp √3×√3 diffraction pattern and in STM the surface showed a good quality, where it was easy to find atomically flat domains with sizes above 250 nm^2. PTCDI was then evaporated using a Knudsen cell held at 275 °C with an evaporation rate of 0.06 ML/min calibrated using a quartz crystal microbalance. The sample was kept at RT during the evaporations. The surface with PTCDI coverages of 0.1, 0.5, 1, 2 and 5 ML were investigated using LEED, STM and STS. STS spectra were recorded on already scanned regions and were made at PTCDI sites by switching off the feedback loop and recording I-V curves. The presented spectra are spatially averages of several molecules in a region. All measurements were done with the sample at RT and all STM bias voltages in the paper are sample-biased.

3 Results

3 a) STM, Sub monolayer coverage:

At 0.1 ML almost all molecules had formed 2D islands as the ones presented in Figure 1. Single molecules and small islands could be found next to defects or step edges, but never on a defect free terrace, indicating that the molecules are very mobile on the substrate. The PTCDI moves to step edges that act as nucleation sites and grow well ordered 2D islands. The islands are structured by rows of PTCDI molecules, where the molecules in alternating rows are oriented slightly differently. The islands usually end with sharp edges parallel to the row direction, and they are elongated along the row direction of the molecules. The angle between the row direction of the islands and the $[11\bar{2}]$ direction of the substrate was measured in STM to be ± (13 ± 0.3)°. Also, because the substrate has 3-fold rotational symmetry the growth direction is not unique. Indeed, islands were also found to have the same ±13° relation to the $[2\overline{11}]$ and $[1\bar{2}1]$ directions. The two islands in Figure 1 have grown together and formed a natural boundary between the two molecular domains. These domains have different orientations as can be seen from the inserted unit cells for each island. Their respective relation to the substrate orientation can be seen from the marked crystal directions in Figure 1.

The rows of differently oriented molecules can clearly be seen in the upper half of Figure 2 a), where each molecule has the shape of a “coffee bean” with two bright sides and a darker central line. In the same image it is clear that the center line is oriented differently for molecules in adjacent rows. The molecular unit cell (MUC) contains two molecules and the two unit vectors were measured to 18.0 Å by 15.6 Å, resulting in an area of 281 $Å^2$. The MUC is not perfectly rectangular and the angle between the two unit vectors is 86 ± 0.5°. It was also

found that molecules in the two types of rows are rotated ± (10 ± 0.4)° with respect to the row direction. The structure described here is presented in Figure 2 b).

Interestingly, at some biases the individual molecules are clearly separated as in the upper part of Figure 2 a), recorded with a sample bias of -2 V. But in other biases the individual molecules in adjacent rows appear to be linked. Looking closely, there are some intensities between molecules in neighboring rows, as one can see in the lower image of Figure 2 a), recorded with sample bias of 0.5 V.

Both in Figure 2 a) and 3 a), some of the molecules are less bright than others. In domains of the 2D islands these darker molecules form rows perpendicular to the molecular row direction. These rows of darker molecules create a superstructure with a distance between the dark rows of 5 molecules along the row direction of the islands, so the superstructure is 5x1 relative to the MUC as shown in Figure 3 a). By using the well resolved substrate in Figure 3 a) a honeycomb chain trimer (HCT) lattice could be fitted to the substrate and consequently the PTCDI molecules could be positioned on the lattice as presented in Figure 3 b). The corner molecules of the superstructure, that appear darker in the STM image, were marked as red ovals while the others were marked as blue ovals. To identify the relation between the 5×1 superstructure unit cell (SUC) and the substrate, the dark rectangle marking the SUC in Figure 3 b) has been isolated in Figure 3 c) together with the $\sqrt{3}\times\sqrt{3}$ unit cell. Now it is possible to identify that SUC involves three repeating units, each having unit vectors with lengths of $\sqrt{39}$ and $\sqrt{21}$ relative to the Si(111)-1×1 unit vector. The SUC is therefore $3\sqrt{39}\times\sqrt{21}$ relative to the Si(111)-1×1 unit cell. Also, because the MUC simply is 1/5 of the SUC in the row direction, the MUC is $(3/5)\sqrt{39}\times\sqrt{21}$ relative to the Si(111)-1×1 unit vector. Using the unit vectors for the SUC, the vectors for the MUC can be calculated to 17.7 Å and 14.4 Å with an

angle between them of 87°. The angle between the row direction and the high symmetry directions was calculated to 13.9°.

Occasionally, in both Figure 2 a) and 3, a few molecules appear even darker than the ones in the dark rows of the superstructure. In the lower image of Figure 2 a) using 0.5 V, these molecules appear to be almost invisible in the STM. But the positions of these “darkest molecules” in the film seem to be random.

3 b) STM, Second Monolayer

The internal structure of the second layer is the same as the first one with islands of two types of rows, but the size of the MUC is slightly different. The in-row vector is now 15.5 Å and the inter-row vector is 17.7 Å, separated by 86 ± 0.5°. The second layer is also rotated 60° relative to the first one and with certain tip conditions a superstructure between the first and the second layer is also observed. Figure 4 a) shows a 2 ML island on top of the first monolayer, together with their respective row direction. In this figure the superstructures for both 1 ML and 2 ML are visible; the 2ML superstructure can be seen as distinct dark spots in the 2 ML island. The growth of the second layer matches the first layer in a point-to-point fashion, which yields the superstructure. The relation between the layers is presented in Figure 4 b), together with the unit cell for the structure. The 2 ML superstructure has a centered unit cell: Its shorter unit vector equals to two times of the 1 ML MUC inter-row vector and its longer unit vector equals to four times of the 1 ML MUC in-row vector. Hence, the 2 ML superstructure is c($2\sqrt{21} \times (12/5)\sqrt{39}$) relative to the Si(111)-1×1 unit vector. It should also be noted that when probing filled states with low biases, it was not possible to resolve individual molecules on the second layer.

3 c) STM, Multilayer

In Figure 5 a) an STM image of a typical multilayer is presented. The preference to grow along the row direction is stronger for coverages above 2 ML. New layers can also begin to grow before the previous layer in that domain is filled. This usually happens when the preferred growth directions are blocked by a domain edge. Above 2 ML no superstructure was found and no island growth was observed for the coverages studied here. For multilayer coverages the STM-measured unit vectors for the structure were 15.6 Å by 17.9 Å, and the angle between them is 87 ± 0.5°. Also, for coverages above 2 ML the growth mode changes so that each layer aligns with the layer underneath in such a way that the unit cell in the upper layers matches with the ones in the lower layers, as can be seen in Figure 5 b). This means that the molecular rows align and molecules are on top of each other. This means that molecular rows and molecules in different layers are on top of each other.

A summary of the STM-measured vectors for unit cells together with the calculated vectors from the superstructures and the DFT calculated “canted” structure by Mura et al. is presented in Table I. Here the vector lengths for the reconstructions have been calculated by multiplying the vectors by the lengths of the Si(111)-1×1 vectors.

3 d) STS

Scanning tunneling spectroscopy was performed when 1, 2 and 5 ML PTCDI had been evaporated onto the sample and the respective spectra are presented in Figure 6. Due to the difficulty in determining the exact coverage of each molecular terrace above 2 ML, the STS made at 5 ML coverage is denoted “multilayer”. Both differential conductance (dI/dV) and normalized dI/dV curves are presented for 1 and 2 ML. Due to the large bandgap in the multilayer spectrum it could not be normalized, and only dI/dV is presented for that coverage.

The dI/dV curves give a general picture of the evolution of the electronic states around the Fermi level, while the normalized dI/dV offers more information about the details close to the Fermi level.

The 1 ML spectrum in Figure 6 a) contains several features. Below the Fermi level there is a small state situated at -0.3 eV and two stronger states at -1.2 eV and -2.5 eV. These three states are tentatively denoted L', H' and H respectively. Above the Fermi level there are two strong features; the first sits at 1.0 eV and is tentatively denoted as L and the other is at 2.7 eV. The normalized 2 ML spectrum presented in Figure 6 b) shows some interesting differences compared to the 1 ML spectrum: Firstly the filled states H and H' are still present and situated at the same energy positions in 2 ML. However the state just under the Fermi level is not present. In the empty-state side there are two states, one at 0.6 eV and one at 2.0 eV which are here denoted L' and L respectively. The dI/dV spectrum for multilayer coverage is presented in Figure 6 c). The only filled state is the previous H state that here has been located at the same energy position as in the previous coverages. In the empty states the feature closest to the Fermi level is a shoulder structure at 1.5 eV, which is denoted L.

3 e) LEED

The LEED image of the substrate in Figure 7 a) shows a sharp $\sqrt{3}\times\sqrt{3}$ pattern. As PTCDI was evaporated onto the substrate a second pattern appears, which at 1 ML PTCDI coverage has comparable strength with the $\sqrt{3}\times\sqrt{3}$ pattern, as can be seen in Figure 7 b). The main features of the PTCDI related pattern are an outer ring and an inner ring with 12 spots and a middle ring with 6 spots. The new pattern has 6-fold symmetry: 3 fold rotational and mirror through the symmetry axes. Weak traces of additional spots around the spots in the outer ring are also visible. For higher PTCDI coverages the substrate related spots disappear but the molecules

related ones remain as in the 2 ML image in Figure 7 c). At 5 ML the pattern is still clearly visible but slightly weaker. To explain the features of the LEED pattern from the STM results, the reciprocal space for the √3×√3 reconstruction, the MUC and the 1 ML SUC are generated and presented in Figure 8. All the main features of the LEED pattern can be explained by spots where the patterns from differently oriented MUC's or SUC's coincide.

4 Discussion

The only sub-monolayer molecular configuration found here was the canted structure with the molecular rows oriented ±13° relative to the high symmetry axes, such as [11$\bar{2}$]. No 1D rows were found in the coverages studied here. This is in good agreement with the results reported by Swarbrick *et al*, [19], where the 2D islands were dominant already at 0.02 ML PTCDI coverage. However, the angles between the row direction and the high symmetry axis were slightly higher in our study compared to the previous one.

The preferred growth direction along the molecular rows is a strong indication that the bond strength in that direction is the dominating interaction in the formation of the 2D structure. This fits well with the stepwise density functional analysis by Mura *et al.* [13], which clearly showed that the strongest possible dimer bonds are the imide mediated hydrogen bonding observed along the rows of the islands. The same DFT study showed that the most stable 2D configuration for the PTCDI molecules is the canted structure found here on Ag/Si(111)-√3×√3. As revealed in Figure 2 and 3, the 1 ML MUC fits very well with the DFT calculated values for the canted structure. Even though the in-row vector is slightly shorter while the inter-row vector is slightly longer than the gas-phase calculated ones, the similarity between PTCDI in gas phase and PTCDI on Si/Ag(111)-√3×√3 is a strong indication that the molecule-molecule interactions is the dominating force in this system. It is however clear that there are some molecule-substrate interactions as evidenced by the 1 ML superstructure.

Figure 3 b) shows that the four corner molecules in the $3\sqrt{39}\times\sqrt{21}$ superstructure are situated so that two Si-trimers are located relatively close to their center axis. These corner molecules have less intensity in STM which shows that the various adsorption sites influences the molecules.

The apparent linking between the molecules in the lower image of Figure 2 a) is a clear evidence of the inequivalent O···H hydrogen bonding among the molecules of neighboring rows. Due to the strong, imide mediated hydrogen bonds, the distance in one diagonal direction of the MUC becomes shorter. O···H hydrogen bonding in this direction seems to be strengthened. Consequently, all the molecules in the shorter diagonal direction are closely linked.

For higher coverages it is apparent that there is a layer-layer interaction and this interaction is strong enough that the preceding layer has an effect on the structure and orientation of the succeeding one. Especially at 2 ML the interaction is strong enough to induce a point-to-point superstructure between the two layers, as illustrated in Figure 4. To our knowledge a molecular layer-layer superstructure visible in STM has not been reported before. At multilayer coverage the layer/layer interaction is such that molecules align on top of each other. Due to the slight difference in STM measured MUC unit vectors for 2 ML and multilayer, one could expect an interface between the second and third layer with a slight mismatch between these two layers. This was not observed in this study, and if there is one, it would be hard to find due to the difficulty in identifying the coverage of each terrace at coverages higher than 2 ML.

The PTCDI related LEED pattern has both mirror- and three-fold rotational symmetry, which fits very well with domains of 2D islands that are oriented ±13.9° relative to the high symmetry directions of the substrate. The generated image of the reciprocal space in Figure 8 shows that the LEED pattern is a combination of the (3/5)√39×√21 MUC and the 3√39×√21 SUC. The spots that are visible in LEED are those where the MUC coincides with the SUC, resulting in the inner and outer ring, or where the two differently oriented SUC patterns coincide, resulting in the middle ring. The fact that the outer ring is the brightest can be explained by the generated image: those spots are where two differently oriented SUCs coincide with the MUC. The weaker spots close to the spots in the outer ring can also be found in the generated image. All in all, the features found in the experimentally obtained LEED pattern can be explained by the structures found in STM and the results from these two experimental techniques fit very well with each other. The fact that the spots in the middle ring are present in the LEED pattern at higher coverage indicates that the 3√39×√21 SUC is present at all coverages even though it was not observed in STM.

The fact that the two vectors of the 1ML SUC are related to the Si(111) 1×1 by vectors involving √21 and √39 is interesting, because structures involving these are quite common on metal/semiconductor √3×√3 reconstructions when extra metal is present. Both the Ag/Ge(111)-√3×√3 and Ag/Si(111)-√3×√3 systems have √39×√39 or √21×√21 reconstructions when different amount of extra Ag or Au is present [16,24,25]. The √21×√21 reconstruction has also been observed when alkali metals have been deposited on the Ag/Si(111)-√3×√3 surface, for instance Na, K and Cs [26–28]. It is apparent that extra atoms on this type of metal/semiconductor surfaces have a preference to arrange themselves into structures with √21 and √39 periodicity and here it is also the case even for layers of a relatively large molecule as PTCDI.

The STS spectra presented in Figure 6 show a remarkable influence of the film thickness on the electronic structure around the Fermi level. Starting with the multilayer spectrum in Figure 6 c), the film thickness when this spectrum was made should be large enough (roughly 5 ML) that influences from the substrate should be negligible, and can therefore be considered as bulk-like. Therefore the H at -2.5 eV and L state at 1.5 eV in Figure 6 c) should be assigned to the bulk-like HOMO and LUMO respectively. This is similar to the result from a combined photoelectron spectroscopy and inverse photoelectron spectroscopy study of a 15 nm thick PTCDI layer on passivated GaAs(100). The energy positions for the HOMO and LUMO in that system were found to be 2.3 eV below- and 1.4 eV above the Fermi level respectively [29].

Comparing the multilayer spectrum to the 1- and 2 ML spectra, it is apparent that the molecule/substrate interaction changes the electronic structure around the Fermi level considerably. There are extra states below the Fermi level (H' and L') and above the Fermi level the states are closer to the Fermi level compared to the bulk-like spectrum. The extra states can be explained by HOMO and LUMO splitting, different molecules interact differently with the substrate and/or surrounding molecules which results in two types of molecules with different electronic structure. This has previously been reported, for instance, for 1 ML PTCDA on Ag(110) [30], Ag(111) [30,31] and Ag/Si(111)-$\sqrt{3}\times\sqrt{3}$ [32]. Also, for 1ML PTCDA on both Ag(110) and Ag(111) the LUMO could be partially filled through charge donations from the substrate, which resulted in a filled state very close to the Fermi level. Comparing this to the 1 ML spectrum in Figure 6 a) H and H' originate from the molecular HOMO that has been split, while L' and L are splits from the molecular LUMO. L' has been filled through charge donation from the substrate and L has moved closer to the Fermi level compared to the bulk-like LUMO. At 2 ML there is still a split but now L' has moved above

the Fermi level and L has moved to 2 eV. In the multilayer spectrum the interaction resulting in the split is no longer present and the L’ and L recombine into the bulk-like LUMO while H’ and H recombine into the bulk-like HOMO.

The HOMO-LUMO levels for the two types may shift due to the different interactions but each individual molecule should still have similar HOMO-LUMO separation. This agrees well with the results here: At 1 ML the H’-L and H-L’ separations are 2.2 eV and 2.3 eV respectively and at 2 ML the separation increases to roughly 3.1 eV for both types. Considering the HOMO-LUMO separation for the film as a whole, the H’-L’ pseudo gap for 1 ML gives a very small value of 0.9 eV. The H’-L’ separation increases to 1.8 eV for 2 ML and for multilayer the bulk-like HOMO-LUMO separation is 4.0 eV.

Summarizing our findings, which complement earlier work of Mura *et al.* and Swarbrick *et al.* we now have a good understanding of the growth of thin PTCDI films on Si/Ag(111)-$\sqrt{3}\times\sqrt{3}$, which involves several stages. For very low coverages the molecules lower their energy by creating rows where the molecules interact through hydrogen bonding mediated by the imide groups. This configuration is energy favorable because the rows are created of the strongest possible dimers. When more molecules are present they can lower the energy further by forming 2D islands with the canted structure. In these islands the oxygen atoms that are not involved in the in-row interaction can approach hydrogen atoms in molecules in adjacent rows, resulting in the two different orientations of molecules in the islands. The first layer interacts with the substrate and creates the $3\sqrt{39}\times\sqrt{21}$ superstructure. The growth of the second ML matches the first ML point-to-point by rotating the second 60 °C relative the first. This results in a c($(12/5)\sqrt{39}\times 2\sqrt{21}$) superstructure in the second layer. Above 2 ML coverage, the layers grow perfectly on top of each other and the layers have less dependence

on the previous layer so that the molecule/molecule interactions become more dominant. The in-row interaction is the strongest, leading to the growth directions along the rows becoming even more dominant for higher coverages. All coverages have the $3\sqrt{39}\times\sqrt{21}$ superstructure because the features in the LEED pattern related to this structure are present in all coverages.

The property of the coverages above 2 ML that the layers align in such a way that the unit cells match each other should result in high π-overlap between the layers, potentially leading to interesting charge transport properties through the film. Another interesting property of this system is the possibility to alter the electronic structure around the Fermi level by carefully adjusting the film thickness. This combined with the single molecular configuration and layer by layer growth could prove this system to be interesting for device applications.

5 Conclusions

Thin films of PTCDI on Ag/Si(111)-$\sqrt{3}\times\sqrt{3}$ were found to grow layer by layer with a single molecular structure that has a $(3/5)\sqrt{39}\times\sqrt{21}$ periodicity relative to Si(111)-1×1. At 1 ML coverage a $3\sqrt{39}\times\sqrt{21}$ superstructure was found in STM and the LEED showed that this structure exists at all coverages. At 2 ML a molecule/molecule induced $c((12/5)\sqrt{39}\times 2\sqrt{21})$ was observed in the STM and for higher coverages the molecular unit cells aligns so molecules lie on top of each other. STS showed that the electronic structure of the system changes considerably with film thickness. At 1 ML the HOMO-LUMO separation is only 0.9 eV and is increased to 1.8 eV for 2 ML thickness. The HOMO-LUMO gap was found to increase further to 4.0 eV for thicker films.

Acknowledgments

The work done here was funded by the Swedish Research Council and the Tage Erlander foundation for science and technology.

References

[1] J. Kwon, M.K. Kim, J.-P. Hong, W. Lee, S. Noh, C. Lee, S. Lee, and J.-I. Hong, Org. Electron. Physics, Mater. Appl. **11**, 1288 (2010).

[2] J. Puigdollers, C. Voz, M. Fonrodona, S. Cheylan, M. Stella, J. Andreu, M. Vetter, and R. Alcubilla, J. Non. Cryst. Solids **352**, 1778 (2006).

[3] P. Peumans, A. Yakimov, and S.R. Forrest, J. Appl. Phys. **93**, 3693 (2003).

[4] V.G. Kozlov, G. Parthasarathy, P.E. Burrows, S.R. Forrest, Y. You, and M.E. Thompson, Appl. Phys. Lett. **72**, 144 (1998).

[5] P. Lin and F. Yan, Adv. Mater. **24**, 34 (2012).

[6] M. Carmen Ruiz Delgado, E.G. Kim, D.A. Da Silva Filho, and J.L. Bredas, J. Am. Chem. Soc. **132**, 3375 (2010).

[7] J.N. O'Shea, A. Saywell, G. Magnano, L.M.A. Perdigão, C.J. Satterley, P.H. Beton, and V.R. Dhanak, Surf. Sci. **603**, 3094 (2009).

[8] L.N. Serkovic Loli, E. a Sánchez, J. Esteban Gayone, O. Grizzi, and V. a Esaulov, Phys. Chem. Chem. Phys. **11**, 3849 (2009).

[9] R. Nowakowski, C. Seidel, and H. Fuchs, Phys. Rev. B **63**, 1 (2001).

[10] J. Hieulle and F. Silly, J. Mater. Chem. C **1**, 4536 (2013).

[11] C. Seidel, A.H. Schäfer, and H. Fuchs, Surf. Sci. **459**, 310 (2000).

[12] J.C. Moreno-López, O. Grizzi, M.L. Martiarena, and E.A. Sánchez, J. Phys. Chem. C **117**, 11679 (2013).

[13] M. Mura, F. Silly, G.A.D. Briggs, M.R. Castell, and L.N. Kantorovich, J. Phys. Chem. C **113**, 21840 (2009).

[14] C. Ludwig, B. Gompf, J. Petersen, R. Strohmaier, and W. Eisenmenger, Zeitschrift Für Phys. B Condens. Matter **93**, 365 (1994).

[15] J.M. Topple, S.A. Burke, S. Fostner, and P. Grütter, Phys. Rev. B - Condens. Matter Mater. Phys. **79**, 1 (2009).

[16] H. Zhang, K. Sakamoto, and R. Uhrberg, Phys. Rev. B **64**, 245421 (2001).

[17] H.M. Zhang, J.B. Gustafsson, and L.S.O. Johansson, Phys. Rev. B **74**, 201304 (2006).

[18] J. Teng, K. Wu, J. Guo, and E. Wang, Surf. Sci. **602**, 3510 (2008).

[19] J.C. Swarbrick, J. Ma, J.A. Theobald, N.S. Oxtoby, J.N. O'Shea, N.R. Champness, and P.H. Beton, J. Phys. Chem. B **109**, 12167 (2005).

[20] J.B. Gustafsson, H.M. Zhang, and L.S.O. Johansson, Phys. Rev. B **75**, 155414 (2007).

[21] D.L. Keeling, N.S. Oxtoby, C. Wilson, M.J. Humphry, N.R. Champness, and P.H. Beton, Nano Lett. **3**, 9 (2003).

[22] J.A. Theobald, N.S. Oxtoby, M.A. Phillips, N.R. Champness, and P.H. Beton, Nature **424**, 1029 (2003).

[23] A. Ishizaka and Y. Shiraki, J. Electrochem. Soc. **133**, 666 (1986).

[24] R.I.G. Uhrberg, H.M. Zhang, T. Balasubramanian, E. Landemark, and H.W. Yeom, Phys. Rev. B **65**, 81305 (2002).

[25] H.M. Zhang, K. Sakamoto, and R.I.G. Uhrberg, Surf. Sci. **532–535**, 934 (2003).

[26] M. D'angelo, M. Konishi, I. Matsuda, C. Liu, S. Hasegawa, T. Okuda, and T. Kinoshita, Surf. Sci. **590**, 162 (2005).

[27] C. Liu, I. Matsuda, H. Morikawa, H. Okino, T. Okuda, T. Kinoshita, and S. Hasegawa, Jpn. J. Appl. Phys. **42**, 4659 (2003).

[28] H.M. Zhang, K. Sakamoto, and R.I.G. Uhrberg, Phys. Rev. B **70**, 245301 (2004).

[29] D.R.T. Zahn, G.N. Gavrila, and M. Gorgoi, Chem. Phys. **325**, 99 (2006).

[30] Y. Zou, L. Kilian, A. Schöll, T. Schmidt, R. Fink, and E. Umbach, Surf. Sci. **600**, 1240 (2006).

[31] L. Kilian, A. Hauschild, R. Temirov, S. Soubatch, A. Schöll, A. Bendounan, F. Reinert, T.L. Lee, F.S. Tautz, M. Sokolowski, and E. Umbach, Phys. Rev. Lett. **100**, 136103 (2008).

[32] H.M. Zhang, J.B. Gustafsson, and L.S.O. Johansson, Chem. Phys. Lett. **485**, 69 (2010).

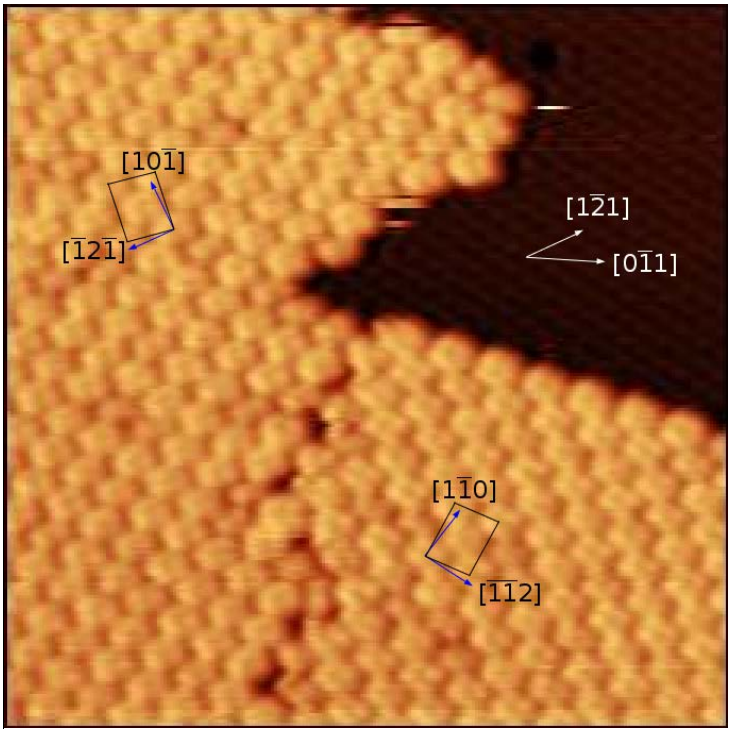

Figure 1 STM image (size 20 nm x 20 nm) taken at -2.0 V and 0.3 nA of PTCDI at sub-monolayer coverage, showing two islands with different orientations. The substrate crystal directions are marked by vectors.

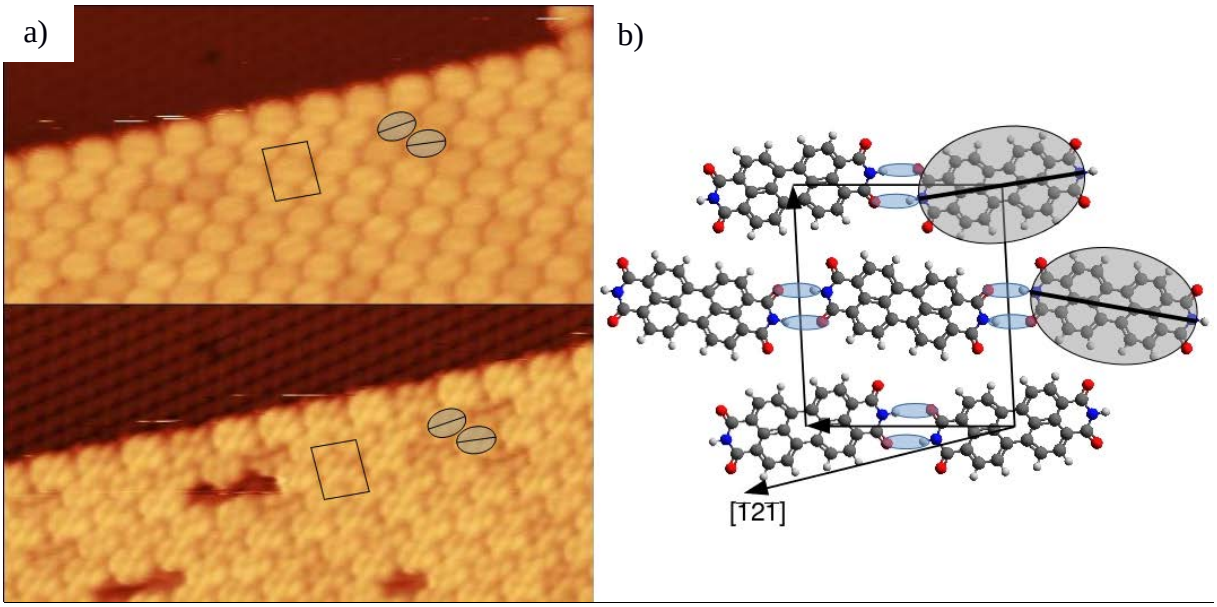

Figure 2 a) STM images (size 10 nm x 20 nm), taken at two different biases (upper -2.0 V and lower 0.5 V), showing the edge of a 2D island. In both images the same unit cell is shown and two PTCDI molecules in neighboring rows are marked as "coffee beans" to illustrate their different orientations. b) Ball and stick model for the 2D structure of the PTCDI islands with the unit cell and its relation to the [$\overline{121}$] substrate direction. The in-row hydrogen bonding are marked in blue and the oval with a central line added to two of the molecules corresponds to the "coffee beans" in a).

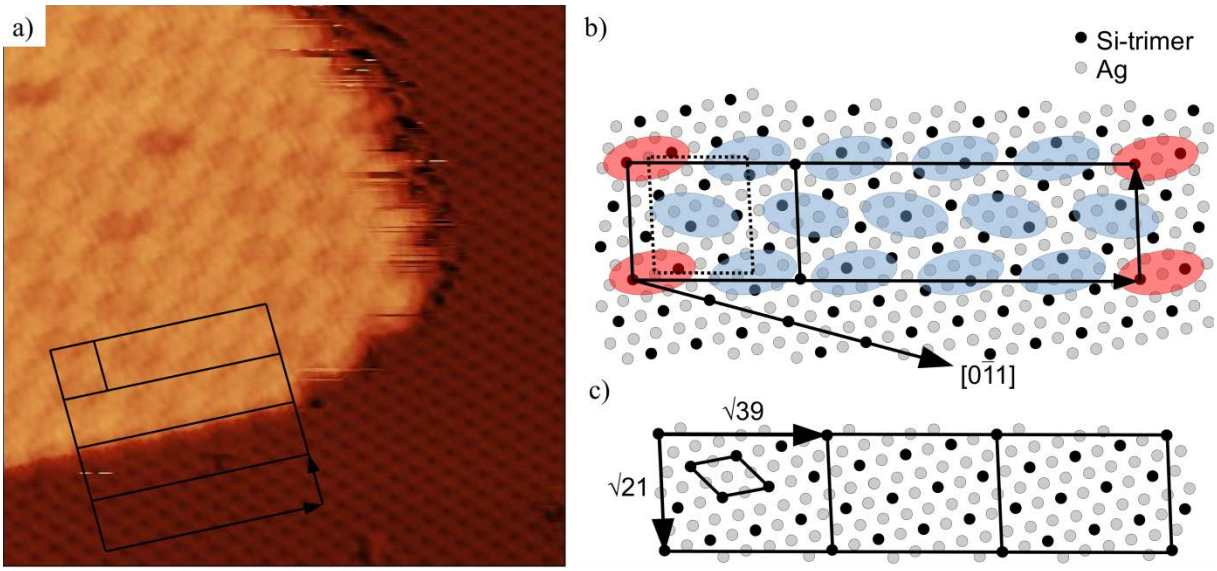

Figure 3 a) STM image (size 20 nm x 20 nm), taken at -2.0 V and 0.3 nA, of a 2D PTCDI 1 ML island and the substrate. The two vectors for the 1ML superstructure, its unit cell and the regular unit cell are shown. b) The HCT model of Ag/Si(111)-√3×√3 substrate with the PTCDI molecules in the 1ML superstructure. The superstructure's dark corner molecules, that appear darker in the STM image in a), are marked as red ovals; the other molecules are marked as blue ovals. c) The three repeating units of the substrate under the superstructure, their lengths relative to the Si(111)-1×1 unit vectors are marked. The small one is the √3×√3 unit cell.

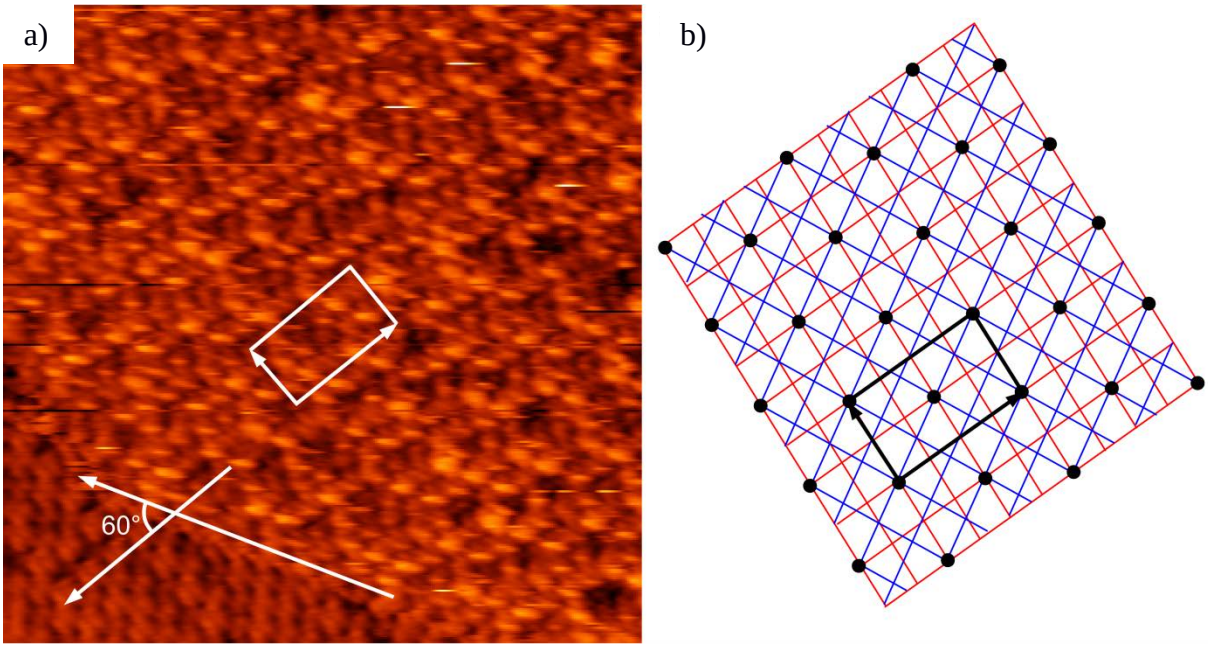

Figure 4 a) STM image (size 30 nm x 30 nm) taken at -2 V and 0.5 nA, of a 2ML PTCDI island with a superstructure. Its unit vectors are shown, as well as 1st and 2nd ML in-row directions. b) An image showing the point-to point growth between the first layer (red) and the second layer (blue).

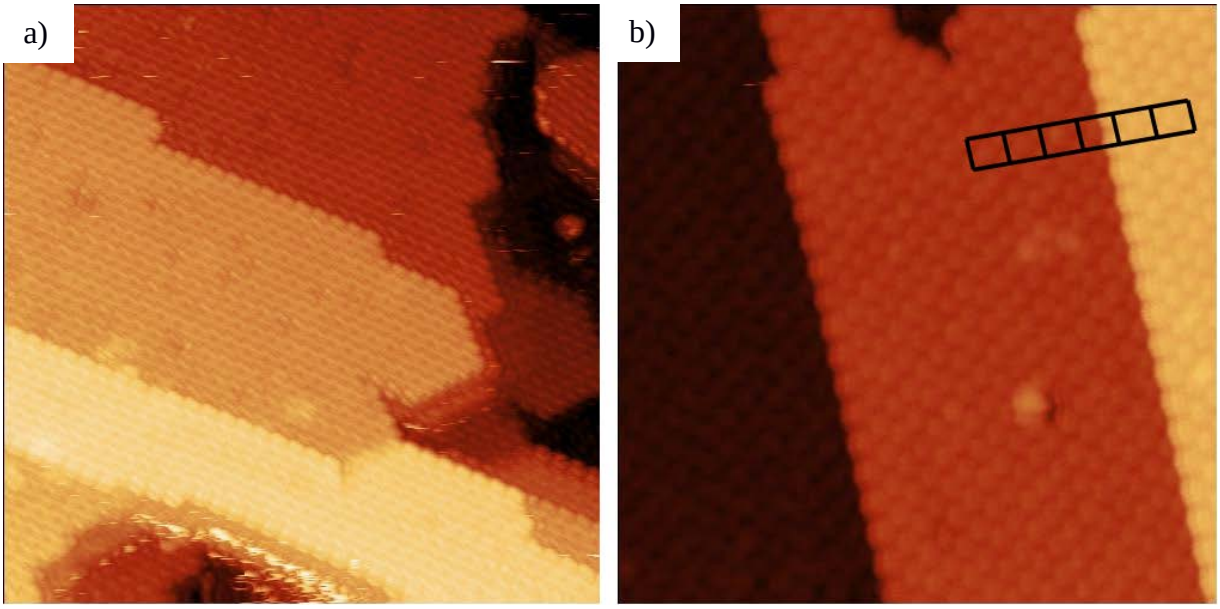

Figure 5a) Typical STM image of multilayer coverage of PTCDI, 2.0 V, 0.3 nA, 50x50nm b) Orientation of layers relative each other for higher coverage than 2 ML, 2.0 V, 0.5 nA, 30x30nm

Table I: Summary of unit vectors and angles (Θ) between them for STM-measured-, Superstructure calculated- and DFT calculated structures at different coverages.

Structure	In-row [Å]	Inter-row [Å]	Θ
1 ML MUC, STM	15.6	18.0	86°
1 ML MUC, (3/5)√39×√21	14.4	17.6	87°
1 ML SUC, 3√39×√21	72	17.6	87°
1 ML MUC, DFT from [1]	14.51	17.45	88.6°
2 ML MUC, STM	15.5	17.7	86°
2 ML SUC, STM*	36.2	60.8	
2 ML SUC, c(2√21 × (12/5)√39)*	35.2	57.6	
Multilayer MUC, STM	15.6	17.9	87°

* The vectors for the 2 ML superstructure do not align with the rows so these are not in-row- and inter-row vectors. The angle between them was not calculated for the same reason.

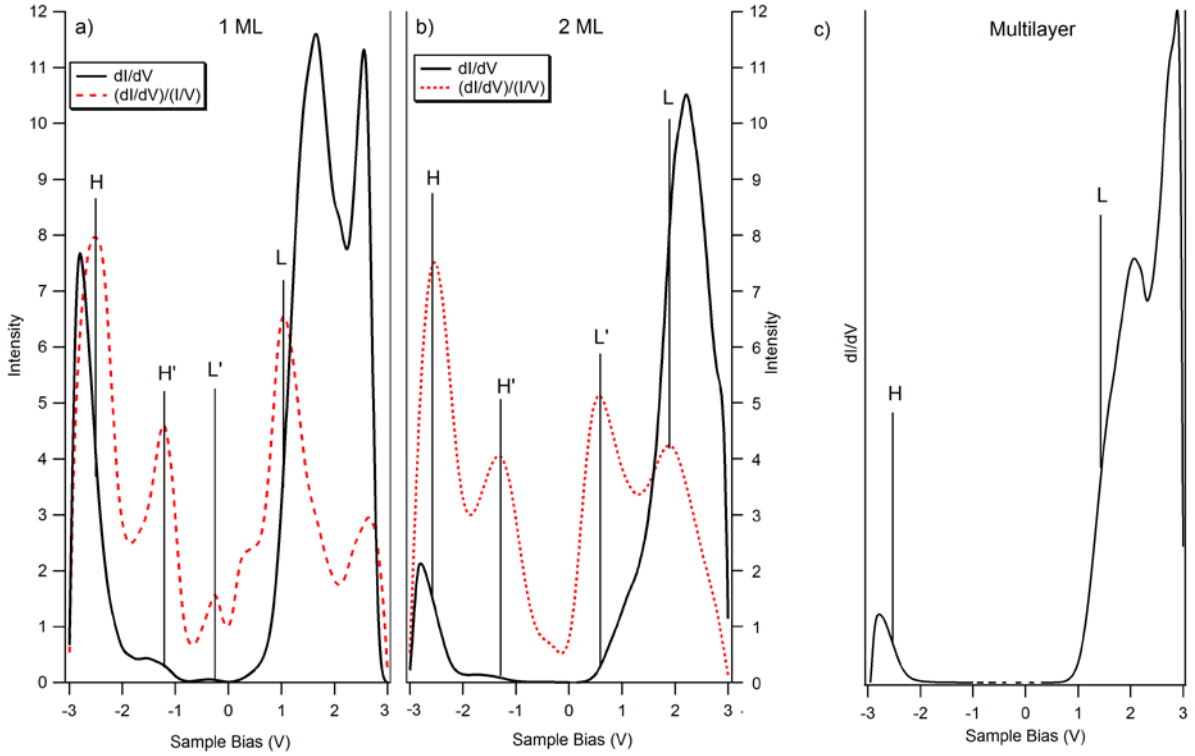

Figure 6 Scanning Tunneling Spectroscopy at different coverages: a) 1 ML b) 2 ML and c) multilayer. The scale in a) and b) is absolute scale for (dI/dV/(I/V)).

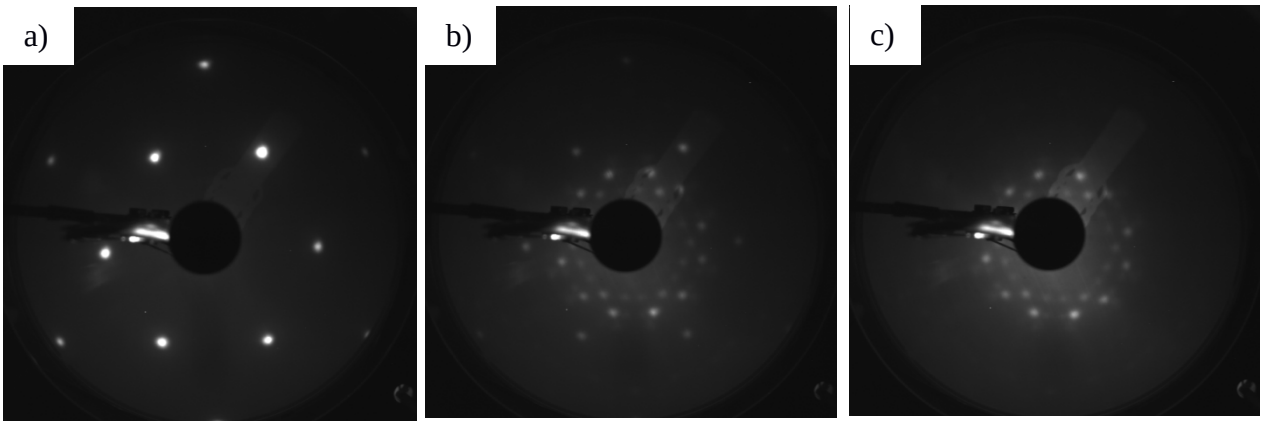

Figure 7 LEED patterns taken at 25 eV acceleration voltage of a) the clean substrate b) 1ML PTCDI c) 2ML PTCDI.

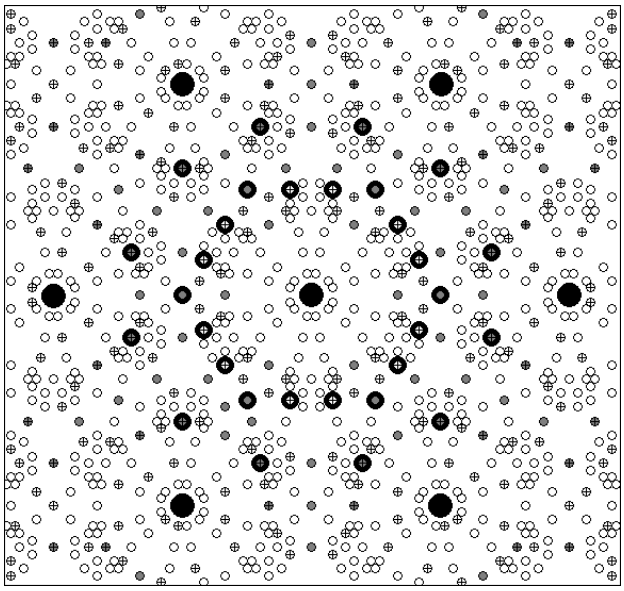

Figure 8 Generated image of the reciprocal space for √3×√3 (big spots), the 3√39×√21 superstructure (rings) and the (3/5) √39×√21 unit cell (crosses). Points where two of the rings for the superstructure coincide are marked with filled rings and the points observed in the LEED pattern have thicker borders.